中國機械工程學刊第四十二卷第三期第 235~244 頁(民國一百一十年)
Journal of the Chinese Society of Mechanical Engineers, Vol.42, No.3, pp 235~244 (2021)

# Effects of Double Pulse Resistance Spot Welding on DP980 Dual Phase Steel

Hwa-Teng Lee * and Yuan-Chih Chang **

**Keywords**： double pulse resistance spot welding, heat affected zone softening, partially melted zone, failure mode.

## ABSTRACT

Multi-step resistance spot welding is an emerging method for the automotive industry that is distinct from conventional one-step resistance spot welding. In this study, one- and two-step resistance spot welding processes were interrogated with respect to tensile-shear tests, weld nugget sizes, hardness distributions, microstructures, and failure modes for different welding parameters. Experimental results reveal that welding nugget size for two-step resistance spot welding was larger than that for one-step resistance spot welding regardless of the welding current. The tensile shear load capacity and the fracture energy for two-step resistance spot welding were better than that for one-step resistance spot welding at lower welding currents. By comparison, at higher welding currents, the tensile shear load capacity and fracture energy were identical for both welding processes because of softening that arises from the higher heat input. Analyses of hardness and microstructure demonstrated that the weldments softened in the partially melted and sub-critical heat-affected zones. Failure mode also depended on the number of pulses that were applied. This study establishes that two-step resistance spot welding increases the extent of softening and alters mechanical properties versus one-step welding due to the greater heat input in the two-step process, especially at higher welding currents.

*Paper Received November, 2020. Revised December, 2020, Accepted December, 2020, Author for Correspondence: Hwa-Teng Lee.*

* *Professor, Department of Mechanical Engineering, National Cheng Kung University, Tainan 701, Taiwan, ROC.*

** *Ph.D. Candidate, Department of Mechanical Engineering, National Cheng Kung University, Tainan 701, Taiwan, ROC.*

## INTRODUCTION

Advanced high strength steel (AHSS) is an important material that is used in the automotive industry to promote efficient energy usage rates and reduce carbon emissions. AHSSs possess stronger mechanical properties than conventional steels and are used in a variety of components in the automotive body. Dual-phase steel, called DP980, is one type of AHSS with higher strength, toughness, and rate of work hardening than conventional high-strength low alloy (HSLA) steels. Moreover, DP980 is amenable to various welding techniques. As a result, dual-phase steel is commonly used in the safety components in automobiles, such as the A- and B-pillars (Kuziak, Kawalla, and Waengler, 2008; Li et al., 2015; Vajragupta et al., 2014; Sirinakorn, Uthaisangsuk, and Srimanosawapal, 2014). Resistance spot welding (RSW) is the most common process for automotive joining because of its stability during welding. Yet, the properties of the welded metal, such as the electrical resistivity and the martensite content, can cause different spot welding performances for AHSS and HSLA. Some studies report that AHSS has a high tendency to produce expulsion that decreases the tensile-shear load and failure energy (Sun, Stephens, and Khaleel, 2008; Pouranvari et al., 2008). Expulsions lead to burrs that increase manufacturing costs, which should be avoided during joining processes. Furthermore, AHSS tolerates a narrower range of welding currents versus HSLA, reducing the welding parameters for this material (Keeler and Kimchi, 2015). Interfacial failure, which is prohibited in tensile-shear tests, tends to occur more frequently in AHSS than in HSLA.

Multi-step resistance spot-welding (RSW) has emerged as a new joining process for automotive steels. This process employs a pulsed welding current such that weldments undergo successive heating and cooling. Hwang et al. (2011) stated that multi-step RSW increases the range of the usable welding currents and reduces the frequency of expulsions. Moreover, the thermal history of weldments could impact failure mode. Several studies demonstrated that spot welding of DP780 and DP980 result in softening of the heat affected zone, which decreases hardness and changes the failure mode (Khan, Kuntz, and Zhou, 2008; Hernandez, Panda, Kuntz, et al., 2010). Xia et al. (2008) concluded that softening increases with the volume fraction of martensite in the steel. AHSS typically contains martensite to promote strength. Therefore, considering the effects of multi-step RSW on the mechanical properties of AHSS is necessary. This study aims to better understand the effects of traditional one-step RSW and two-step RSW on the mechanical properties, microstructures, and failure modes of DP980.

## EXPERIMENTAL PROCEDURES

This study used uncoated dual phase steel DP980 (1.2 mm thick), the chemical compositions of which are listed in Table 1. An experiment was performed to estimate the welding current and confirm the current range. This experiment used different weld currents to obtain the corresponding nugget diameters, and the interval for each weld current was set as 0.4 kA from the starting weld current 4.5 kA to the ending weld current 7.7 kA, as shown in Figure 1. AWS D8.1M was used to standardize the feasible current for automotive spot welding. The left limit of the welding nugget size is $4t^{0.5}$, where $t$ is the sheet thickness in millimeters, at the minimum current. The use of welding currents below the minimum current yielded smaller nugget sizes, resulting in insufficient mechanical properties. The right limit of the welding current is defined as the current at which expulsion occurs. The range of currents for welding was established to be 4.9 to 7.3 kA. The welding time was fixed at 250 ms and three current values of 5.5, 6.0, and 6.5 kA were used to evaluate the effects of low to high heat input.

Table 1. Chemical compositions of DP980

| Element | C | Si | Mn | P | S | Fe |
|---|---|---|---|---|---|---|
| wt% | 0.10 | 0.10 | 1.96 | 0.012 | 0.002 | Bal. |

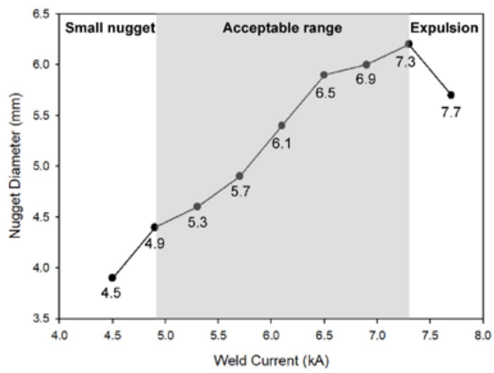


Fig. 1. Plot of nugget diameter versus welding current range for DP980 materials.

One- or two-step RSW were used as joining processes, as shown in Figure 2. The two-step RSW used a preheating current of 6.0 kA, while the one-step RSW did not. An electrode force of 400 kgf was applied for both processes, and the squeeze, weld, and holding times were 1000, 250, and 200 ms, respectively. A complete list of the welding parameters is shown in Table 2. An intermediate frequency direct current (DC) welding machine (NASTOA CO., LTD., Tokyo, JAPAN) with Cu-Cr-Zr alloy electrodes was used, and the DC inverter has the max capacity of 480 kVA and the rated capacity of 173 kVA. The electrodes had truncated cone tips with a 6 mm diameter and were cooled by a continuous circulating flow of water.

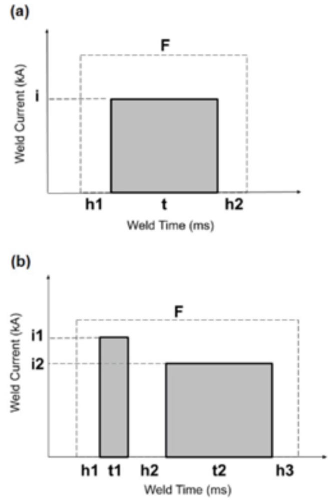


Fig. 2. Schematic diagrams of pulse schedules for (a) one-step (b) two-step RSW processes.

Table 2. Parameters for RSW processes

| **One-Step Process** | | |
|---|---|---|
| **F** | Weld force, kgf | 400 |
| **h1** | Squeeze time, ms | 1000 |
| **t** | Weld time, ms | 250 |
| **h2** | Holding time, ms | 200 |
| **i** | Weld current, kA | 5.5, 6.0, 6.5 |
| **Two-Step Process** | | |
| **F** | Weld force, kgf | 400 |
| **h1** | Squeeze time, ms | 1000 |
| **t1** | Preheat weld time, ms | 60 |
| **h2** | Holding time, ms | 15 |
| **t2** | Weld time, ms | 250 |
| **h3** | Holding time, ms | 200 |
| **i1** | Preheat weld current, kA | 6 |
| **i2** | Weld current, kA | 5.5, 6.0, 6.5 |

The tensile shear test is a convenient method to evaluate the loading capacity of weldments and thus was used in our study. The dimensions of the test specimens were 105 mm × 45 mm with an overlap length of 35 mm, and the schematic is shown in Figure 3. Tensile shear tests were performed by using a 100-kN capacity GOTECH AI-7000 material testing system with a crosshead speed of 5 mm/min. These tests established the tensile-shear load, while the fracture energy was calculated from the stress–strain curve. Hardness measurements were conducted by using a Vickers hardness tester with a load of 500 g for 10 s. Microstructures were probed by using an optical microscope (LEXT OLS 410) and scanning electron microscope (Zeiss sigma 300) on samples that were ground, polished, and etched (with 2-percent Nital) following standard metallographic procedures. Failure mode was analyzed by using an optical microscope (OLYMPUS DSX 110).

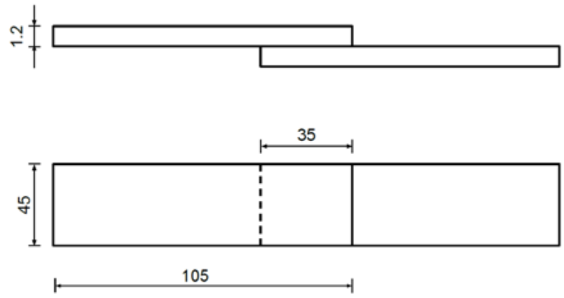


Fig. 3. Schematic diagram of tensile-shear test samples (unit: mm).

## RESULTS AND DISCUSSION

### Nugget diameter investigation of the weld specimen

Figure 4 shows the changes in the weld nugget diameters of DP980 that result from one-step and two-step RSW at welding currents of 5.5, 6.0, and 6.5 kA. The nugget diameter increases with higher welding current for both processes, but the two-step RSW produces larger nugget diameters than the one-step RSW.

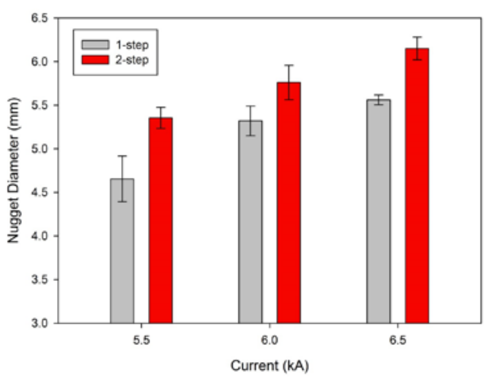


Fig. 4. Dependence of DP980 nugget diameter on weld currents from 5.5 to 6.5 kA for (gray) one-step and (red) two-step RSW.

The welding current is related to the heat input by the relationship defined in Joule's law, which is $H = I^2Rt$. Here, $I$ refers to the current, $R$ is the resistance, and $t$ is time. This equation establishes that the heat input increases with the square of the current, such that increasing current substantially raises heat input. Rao et al. (2017) and Lin et al. (2018) showed that greater heat input during welding promoted the growth of the nugget diameter. Thus, nugget diameter increases with welding current. In this study, while identical welding currents were used for the one-step and two-step RSW, the additional preheating welding current used in the two-step RSW provides greater heat input. This explains the observation of larger weld nugget diameters for the two-step RSW versus one-step RSW.

### Mechanical properties in the tensile-shear test

Figure 5(a) shows the variation of tensile-shear load in DP980 prepared by using different welding currents. The tensile-shear load of materials subjected to the two-step RSW is higher than those prepared by the one-step RSW at welding currents of 5.5 and 6.0 kA. But tensile-shear load is statistically identical when 6.5 kA welding currents were used. Similarly, the fracture energies of materials prepared by the two-step RSW are higher than for those prepared by the one-step RSW at 5.5 and 6.0 kA, but identical when 6.5 kA currents were used, as shown in Fig. 5(b).

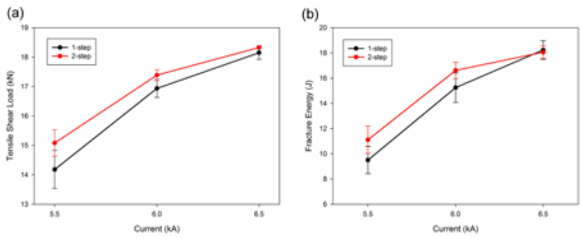


Fig. 5. Mechanical properties of materials prepared by one-step and two-step RSW, specifically (a) tensile shear load and (b) fracture energy.

To summarize, higher welding currents increase nugget diameter due to the greater heat input, while the increased nugget diameter promotes higher loading capabilities and fracture energies. Liu et al. (2012) established a positive linear correlation between nugget diameter and tensile-shear load. Pouranvari (2011) also found that the fracture energy of the weldment increased with the nugget diameter. These corroborate our observations that materials prepared by two-step RSW at currents of 5.5 and 6.0 kA have higher tensile-shear loads and higher fracture energies versus materials prepared by one-step RSW. However, at a welding current of 6.5 kA, the tensile-shear load and the fracture energy of the two-step RSW are identical to that of the one-step RSW. Although the two-step RSW promotes larger nugget diameters, which correlate enhanced tensile-shear load and the fracture energy, this trend is observed. Radakovic et al. (2008) utilized finite element methods to simulate the failure behavior of resistance spot weldments during tensile-shear tests. They found that the material strength has strong correlation with the nugget diameter whatever the failure mode is. VandenBossche (1977) used mechanics of materials to derive the expressions for the equivalent tensile stresses, and the results showed that the nugget diameter was an important factor in each failure mode. In other words, there might be additional factors that can influence the mechanical properties of welded steels besides the nugget diameter, which are discussed in the following sections.

**Hardness measurement of the weld specimen**

Figure 6 shows the distribution of hardnesses for weldments prepared by the one- and two-step RSW. The trend of hardness distribution is nearly identical for both processes. Specifically, the base metal (BM) exhibits a hardness of HV320 on average, while the fusion zone (FZ) has a higher hardness of approximately HV400. The curve in Figure 6 shows a characteristic drop in hardness that occurs in the partially melted zone (PMZ) and the sub-critical heat affected zone (SCHAZ) of the heat affected zone (HAZ). Figure 7 displays the microstructure of the weldment prepared by two-step RSW. The microstructure can be further classified based on the extent of the heat input into five zones: the partially melted zone (PMZ), coarse-grain heat affected zone (CGHAZ), fine-grain heat affected zone (FGHAZ), inter-critical heat affected zone (ICHAZ), and the sub-critical heat affected zone (SCHAZ).

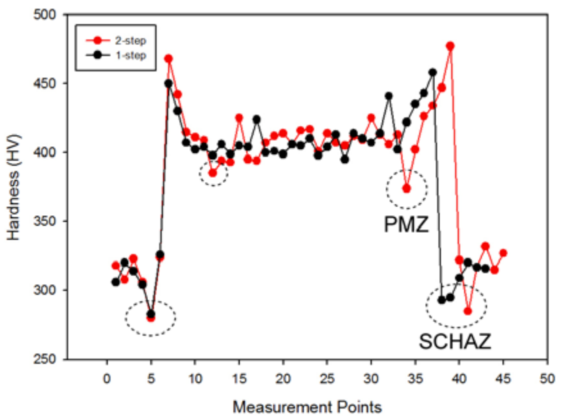


Fig. 6. Distribution of hardness in weldments prepared by using weld currents of 6.5 kA and either (black) one-step and (red) two-step RSW.

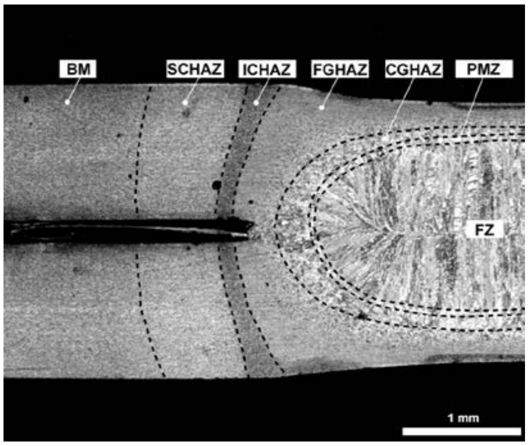


Fig. 7. Optical image that shows various macrostructures region in this material specimen.

Figure 8 shows the hardness of the PMZ, which is adjacent to the FZ, for the sample that was welded by using the two-step RSW at 6.5 kA. The diamond-like indentations indicate the distribution of hardness from the FZ to the HAZ, including the PMZ. The PMZ has a relatively lower hardness (HV374) than the FZ (HV412, HV406, and HV413) and HAZ (HV401 and HV426). The lower hardness results in the relatively lower strength of the PMZ. The dashed line represents PMZ, which was identified by hardness and microstructure. Figure 9 shows the hardness of the SCHAZ in materials prepared by one- and two-step RSW with different weld currents. The SCHAZ of materials produced by one-step or two-step RSW at 5.5 and 6.0 kA have statistically identical hardnesses, whereas two-step RSW produces SCHAZ with comparatively lower hardness when using welding currents of 6.5 kA. Namely, the mechanical properties decline with higher heat input, i.e. at the 6.5 kA welding current. Mechanical property measurements reveal two soft regions with relatively low hardnesses that are located in the HAZ of the DP980 weldment. Specifically, these regions are the PMZ in the HAZ that is adjacent to the FZ and the SCHAZ in the HAZ that is adjacent to the BM.

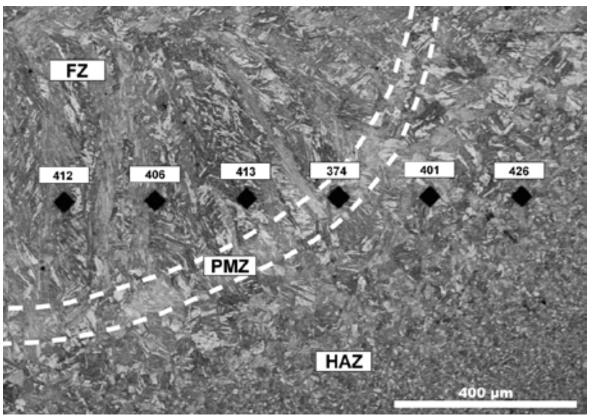


Fig. 8. Distribution of hardness nearby the PMZ for materials prepared by using a current of 6.5 kA and two-step RSW.

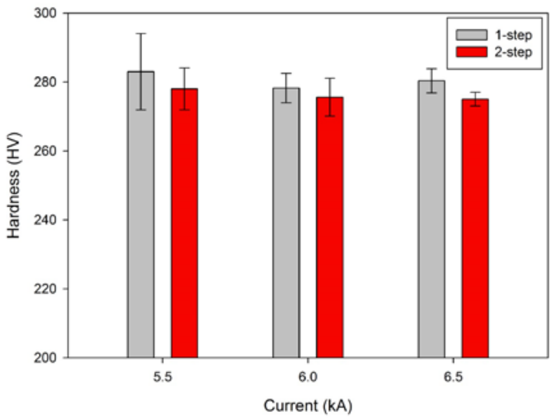


Fig. 9. Hardness of the SCHAZ for materials prepared by using (gray) one-step and (red) two-step RSW.

The properties and dimensions of the PMZ are influenced by welding conditions. Chabok et al. (2018) concluded that two-step RSW has two key effects on the properties of the PMZ. First, the PMZs of materials prepared by two-step RSW have lower densities of high-angle grain boundaries. Second, higher heat input eliminates the compressive stress perpendicular to the plane of the crack, which ultimately reduces residual stress in the PMZ. Huang et al. (2001) proposed an equation that relates the dimensions of the PMZ and to the welding conditions, which showed that a more shallow temperature gradient results in a wider PMZ. In our study, the two-step RSW had a greater heat input and yielded a wider PMZ. By comparison, the one-step RSW had a narrower PMZ. Thus, materials prepared by two-step RSW may have weaker resistances to crack propagation than those prepared by one-step RSW. Moreover, cracking is more easily triggered in the PMZ because of the reduced hardness.

The SCHAZ in the HAZ is another soft region in the DP980 weldment. Zhang et al. (2011) showed that the strength of the weldment can be improved by enhancing the tensile and yield stress in the HAZ. Zhou et al. (2003) used a finite element method to interrogate the loading behavior of the HAZ, which revealed that the mechanical properties of the HAZ had a strong relationship with those of the weldment. Our results show no obvious differences in the degree of softening of the SCHAZ in materials prepared by one- and two-step RSW at currents of 5.5 and 6.0 kA, as evidenced by the near indistinguishable hardnesses of these materials. But at welding currents of 6.5 kA, the hardness of the SCHAZ prepared by two-step RSW was lower than that of the one-step RSW, resulting in poorer mechanical properties. Ultimately, a softer SCHAZ is detrimental to the tensile-shear strength and facilitates crack formation.

**Microstructure investigation of the weld specimen**

As discussed above, the regions of the spot-welded materials can be classified into the BM, HAZ, and FZ based on the influences of heat. The complicated thermal history of the HAZ prompted further subdivision of the HAZ into the CGHAZ, FGHAZ, ICHAZ, and SCHAZ, as shown in Figure 7. Figure 10 shows high-magnification optical images of the microstructures in the various regions. The optical image of the microstructure in the FZ (Figure 10(a)) reveals epitaxial growth of the solidified grains towards the weld center and the formation of martensite, specifically at locations where the temperature exceeds the liquidus temperature and subsequently rapidly cools by heat dissipation. Shrinkage and solidification cracks are the two key welding defects in the FZ area. Joaquin et al. (2007) believed that improper welding parameters cause shrinkages. Ma et al. (2008) discovered that cracks are caused by volume shrinkage in the weldments of dual phase steels. Figure 10(b) shows the microstructure in the PMZ. This region is located at the junction of FZ and HAZ, and the temperature of this area passes through the solid-liquid mixing zone (also called the mushy zone) during the welding processes. Visualization by the optical microscope shows whitening in the PMZ. The image in Figure 10(c) depicts the microstructure of the CGHAZ which experiences a higher temperature region of the austenite phase above Ac3. Coarse austenite transforms into martensite after rapid cooling to yield coarse grains. The FGHAZ experiences temperatures that are above the Ac3 but slightly lower than those experienced by the CGHAZ, resulting in finer austenite grains and subsequent transformation to finer martensite, as shown in Fig. 10(d). The microstructure of the ICHAZ originates from temperatures that reach between Ac1 and Ac3. The industrial production of a DP980 is mostly performed by intercritical annealing and, thus, the ICHAZ microstructure is similar to the microstructure of the BM. Figure 10(e) shows the microstructure in the ICHAZ, which is composed of a mixture of bright ferrite (F) and gray martensite (M). Figure 10(f) shows the microstructure in the SCHAZ, which indicates that the temperature of this region was below Ac1 and no phase transformation, but rather a tempering effect. Therefore, the structure is tempered martensite with a large quantity of scattered, precipitated carbides. The base metal does not experience any heating and the microstructure is shown in Fig. 10(g). A small number of carbides are present because the martensite-start (Ms) temperature of the DP980 is above room temperature and undergoes self-tempering as the cooling is completed.

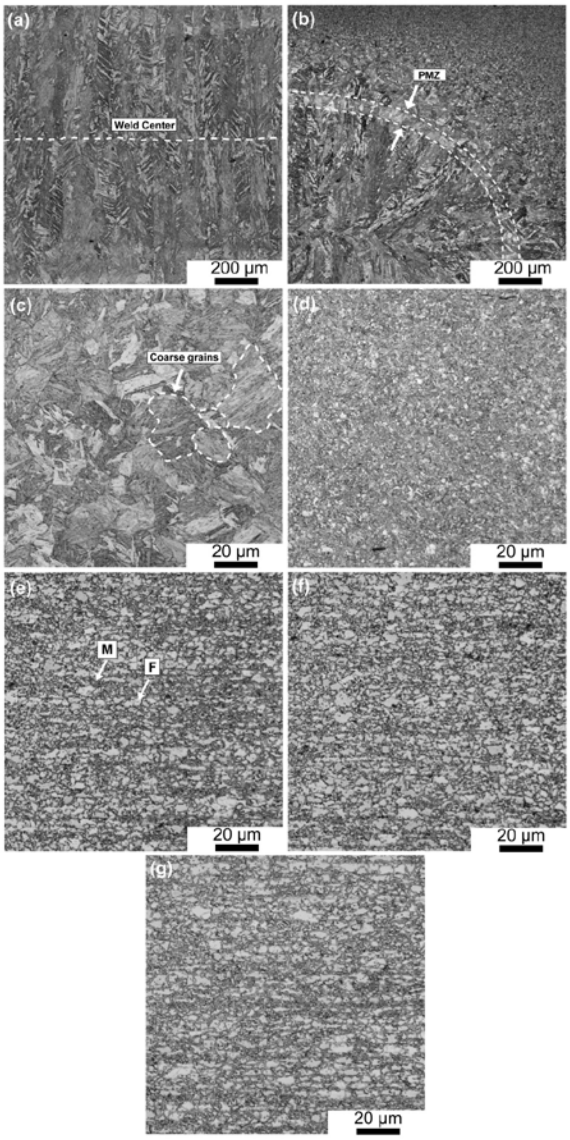


Fig. 10. Optical images that depict various microstructures at various regions in the material specimen, specifically the (a) FZ, (b) PMZ, (c) CGHAZ, (d) FGHAZ, (e) ICHAZ (f) SCHAZ, and (g) BM.

The PMZ thermal history of DP980 cools through the two-phase (the liquid phase and the δ ferrite) region. At equilibrium or with very slow cooling of the alloy through the peritectic temperature, the liquid phase reacts with the δ phase to produce a γ phase. But the rapid solidification in spot welding processes is a non-equilibrium phenomenon. Zhao et al. (2018) reported that during spot welding, the two-phase region would produce segregation because of the redistribution of solute, resulting in a different phase composition. The image in Figure 11(a) captures the microstructure near the PMZ, with the characteristically white PMZ marked with a dashed line. An enlarged view of the PMZ is shown in Figure 11(b), which bears the indentation of a microhardness test. The grain boundary of the PMZ is marked with a dashed line. The original hardness of the same crystal grain is HV387, but the hardness outside of the PMZ (defined by the dashed line) declined to HV310. The SEM image in Figure 12 reveals the morphology of the PMZ, and importantly exhibits the presence of ferrite, which is gray, located adjacent to the prior austenite grain boundary (γ-GB). Thus, these results indicate that softer phases may cause a decline in the hardness of the PMZ. This is corroborated by a study by Soomro et al. (2019) that reports similar results after applying double pulse RSW on HSLA, which formed ferrite on the periphery of the FZ during two-step RSW.

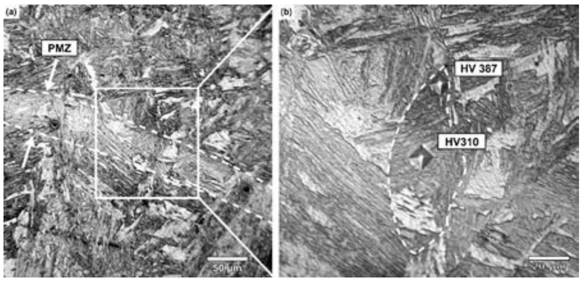


Fig. 11. Microhardness in different zones under optical microscope from an (a) overall view, (b) enlarged view of a particular subsection.

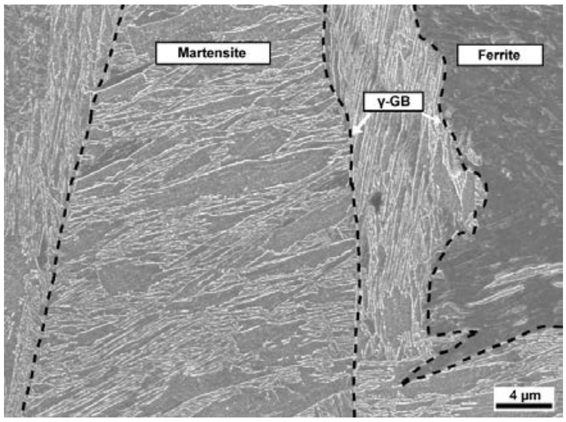


Fig. 12. SEM images that depict the microstructure in the PMZ.

The presence of tempered martensite in the SCHAZ is thought to be the major cause of decreased hardness (Hernandez, Panda, Kuntz, et al., 2010; Hernandez, Panda, Okita, et al., 2010). Thus, the volume fraction of martensite and the degree of tempering could promote a softening effect. Khan et al. (2008) noted that greater volume fractions of martensite increase the degree of softening. Farabi et al. (2011) interrogated laser welding of dissimilar materials between DP600 and DP980 and discovered that DP980 had greater softening because the martensite content of DP980 (about 50 volume percent) was greater than that of DP600 (about 20 volume percent). Pouranvaria et al. (2011) indicated that greater heat input would raise the degree of tempering, which would indicate that the two-step

RSW would have a greater softening effect than the one-step RSW. Figure 13 presents the microstructure of the SCHAZ in materials prepared by the two-step RSW. The structure is composed of ferrite (gray color in Figure 13) and tempered lath martensite (white color in Figure 13). A severely tempered structure is clearly observed and originates from the tempering effects and subsequent decomposition of martensite. The image in Figure 13 also indicates the presence of several continuous carbides and fine carbide precipitates at the grain boundaries, packet boundaries, and block boundaries. Some studies (Pouranvari, Marashi, and Safanama, 2011; Hernandez, Nayak, and Zhou, 2011) have demonstrated that rapid cooling of non-isothermal tempering, which occurs during spot welding, delays the formation of spheroidized carbides and recrystallization processes. By comparison, more fine carbides were precipitated. Biro et al. (2010) also reported that greater heat inputs cause more severe decomposition of martensite. Consequently, two-step RSW increases the heat input and alters the microstructure of the SCHAZ as compared to one-step RSW, ultimately resulting in decreased hardness and tensile-shear strength.

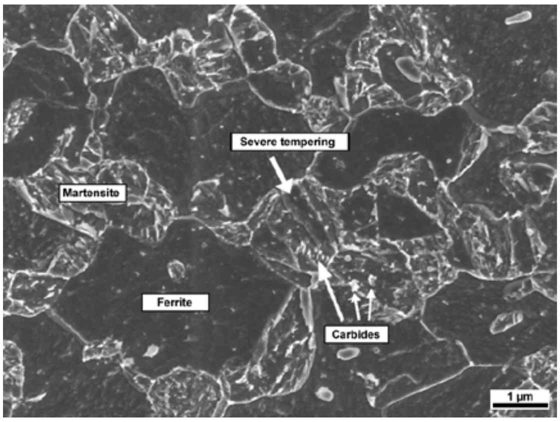


Fig. 13. SEM images of the microstructure in the SCHAZ.

**Failure mode analysis after the tensile-shear test**

The failure mode of weldment fracture is related to heat input. In our study, DP980 exhibited three distinct types of failure modes. Figure 14(a) illustrates an interfacial failure (IF) mode in which a flat fracture surface separates the weld nugget. The partial thickness-partial pullout (PT-PP) failure mode results in characteristic visible features on the weld nugget, which are shown in Figure 14(b). Figure 14(c) depicts a pullout failure (PF) mode, in which the fracture occurs at a peripheral position while the weld nugget remains jointed. A clearer image of PF is presented in Figure 14(d), which shows a side view that highlights the torsional features of PF that arise from tensile shear testing. Figure 15 shows the failure modes of materials prepared using different currents by both one- and two-step RSW. Materials prepared by using a current of 5.5 kA (ref. Figure 15(a), (b)) fail by IF modes, regardless of whether one- and the two-step RSW were used. Similarly, materials prepared by using one-step RSW with a current of 6.0 kA exhibit an IF failure mode, but those prepared at the same current with two-step RSW fail by PT-PP mode (ref. Figure 15(c), (d)). Finally, materials prepared by one-step or two-step RSW at a current of 6.5 kA (ref. Figure 15(e), (f)) fail by PT-PP and PF modes, respectively.

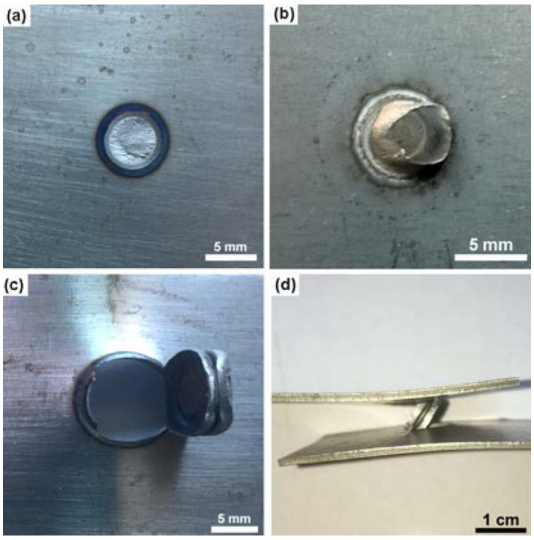


Fig. 14. Optical images of macrostructures that underwent various failure modes, in particular (a) IF, (b) PT-PP, (c) PF, and (d) the side view of PF.

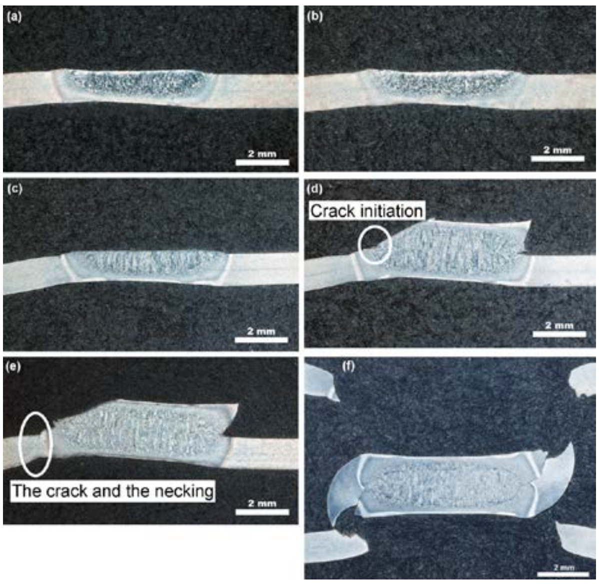


Fig. 15. Optical images of macrostructures that exhibit failure. Images are of materials prepared by using an (a) 5.5 kA weld current with one-step RSW, (b) 5.5 kA weld current with two-step RSW, (c) 6.0 kA weld current with one-step RSW, (d) 6.0 kA weld current with two-step RSW, (e) 6.5 kA weld current with one-step RSW, (f) 6.5 kA weld current with two-step RSW.

Pouranvaria et al. (2007) noted that weldments are simultaneously subjected to both shear and bending forces during tensile shear tests, which would prompt the weldment to rotate and align with the direction of applied force. Cracks initiated at the joint of the two plates that were adjacent to the weld nugget, due to the concentration of stress by the notch effect (Pouranvari and Marashi, 2012), as shown in Figure 15(d). However, the crack with severe necking began in the SCHAZ during high heat input, as illustrated in Figure 15(e). According to the discussion above, the directions of both initiation and propagation of the crack can be determined. Figure 16 displays a scheme of the failure mode for spot welding of DP980. At low heat inputs, the weld nugget is too small to bear shear loading. Therefore, the concentration of stress causes the crack to start from the tip and propagate along the welding center, as shown in Path 1 in Figure 16. As heat input increases and the weld nugget grows, the weldment tends to rotate as a result of torque and is subjected to tensile stress. Hence, cracks would likely propagate along the PMZ because of lower crack resistance in this direction, as shown in Path 2 in Figure 16. At much higher heat inputs, cracking mainly originates from tensile stress. Cracks initiate and propagate in the SCHAZ, which is the region with the lowest hardness in the weldment, as shown in Path 3 in Figure 16. Sun et al. (2008) demonstrated that PF has a larger capacity for loading and energy absorption than IF. In our study, nonetheless, the greater heat input of the two-step RSW changes the microstructure of the HAZ and PMZ, causing a change in the failure mode. Accordingly, at a welding current of 6.5 kA that provides even higher heat input, the failure mode is PT-PP for materials prepared by one-step RSW, but PF in those prepared by two-step RSW due to softening in the SCHAZ. The change of the failure mode eventually impacts the tensile shear loading and energy absorption.

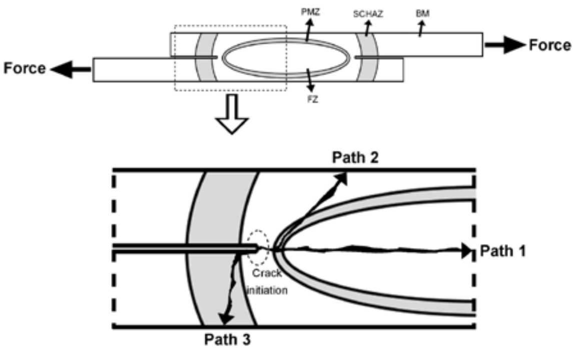


Fig. 16. Schematic illustration of failure modes in AHSS that occur along different paths.

## CONCLUSIONS

Two-step RSW is an emerging spot welding process in the automotive industry. Here, we interrogated in detail the effects of two-step RSW on the mechanical properties of DP980, which is a commonly used material for automotive manufacturing. Our results support the following key conclusions:

1. Two-step RSW not only increases the width of the weld nugget but also influences the extent of softening. Greater softening may change mechanical properties, which is demonstrated by tensile shear tests and the measurements of fracture energy. The tensile shear load and fracture energy of materials prepared by using two-step RSW were better than those of materials prepared by one-step RSW at weld currents of 5.5 and 6.0 kA. However, the tensile shear load and fracture energy of materials prepared by both RSW processes were identical at 6.5 kA. The change in the trend is attributed to softening effects.
2. Softening of the PMZ and SCHAZ are two mechanisms that influence the tensile-shear load and fracture energy of weldments. Softening of the PMZ arises from the presence of ferrite formed by rapid cooling, while the softening of the SCHAZ originates from the tempered martensite that is formed by thermal effects. For two-step RSW, the size of the PMZ increases with more shallow temperature gradients. Moreover, the heat input can also increase the extent of softening, which induces further decomposition of the tempered martensite.
3. In DP980 materials prepared by both one- and two-step RSW, the failure mode changes with heat input. For lower heat inputs, the failure mode is IF and cracks propagate along the center line of the weld. At higher heat inputs, fractures occur in the PMZ due to lower hardness, which leads to PT-PP type failure. Materials prepared with the largest heat input show softening in the SCHAZ that result in PF.
4. Multi-pulse spot welding is a new process for preparing advanced high strength steel in the automotive industry. Yet, additional pulses increase the heat input and change the microstructure of the material, which can impact the mechanical properties of the weldment by softening of the PMZ and SCHAZ.

## REFERENCES

Biro, E, JR McDermid, JD Embury, and Y Zhou, “Softening kinetics in the subcritical heat-affected zone of dual-phase steel welds”, *Metallurgical and materials* *transactions A*, Vol. 41, No. 9, pp. 2348-2356 (2010)

Chabok, Ali, Ellen van der Aa, Indranil Basu, Jeff De Hosson, and Yutao Pei, "Effect of pulse scheme on the microstructural evolution, residual stress state and mechanical performance of resistance spot welded DP1000-GI steel", *Science and Technology of Welding and Joining*, Vol. 23, No. 8, pp. 649-658 (2018)

Farabi, N., D. L. Chen, and Y. Zhou, "Microstructure and mechanical properties of laser welded dissimilar DP600/DP980 dual-phase steel joints", *Journal of Alloys and Compounds*, Vol. 509, No. 3, pp. 982-989 (2011)

Hernandez, VH Baltazar, SK Panda, ML Kuntz, and Y Zhou, "Nanoindentation and microstructure analysis of resistance spot welded dual phase steel", *Materials Letters*, Vol. 64, No. 2, pp. 207-210 (2010)

Hernandez, VH Baltazar, SS Nayak, and Y Zhou, "Tempering of martensite in dual-phase steels and its effects on softening behavior", *Metallurgical and Materials Transactions A*, Vol. 42, No. 10, pp. 3115 (2011)

Hernandez, Victor Hugo Baltazar, Sushanta Kumar Panda, Yasuaki Okita, and Norman Y Zhou, "A study on heat affected zone softening in resistance spot welded dual phase steel by nanoindentation", *Journal of Materials Science*, Vol. 45, No. 6, pp. 1638-1647 (2010)

Huang, C, and S Kou, "Partially melted zone in aluminum welds-planar and cellular solidification", *Welding Journal*, Vol. 80, No. 2, pp. 46-53 (2001)

Hwang, In Sung, Mun Jin Kang, and Dong Cheol Kim, "Expulsion reduction in resistance spot welding by controlling of welding current waveform", *Procedia Engineering*, Vol. 10, No. pp. 2775-2781 (2011)

Joaquin, ARMANDO, Adrian NA Elliott, and CHONGHUA Jiang, "Reducing shrinkage voids in resistance spot welds", *WELDING JOURNAL-NEW YORK-*, Vol. 86, No. 2, pp. 24 (2007)

Keeler, Stuart, and Menachem Kimchi. 2015. *Advanced high-strength steels application guidelines V5*: WorldAutoSteel.

Khan, MI, ML Kuntz, and Y Zhou, "Effects of weld microstructure on static and impact performance of resistance spot welded joints in advanced high strength steels", *Science and Technology of Welding and Joining*, Vol. 13, No. 3, pp. 294-304 (2008)

Kuziak, R., R. Kawalla, and S. Waengler, "Advanced high strength steels for automotive industry", *Archives of Civil and Mechanical Engineering*, Vol. 8, No. 2, pp. 103-117 (2008)

Li, Chang-sheng, Zhen-xing Li, Yi-ming Cen, Biao Ma, and Gang Huo, "Microstructure and mechanical properties of dual phase strip steel in the overaging process of continuous annealing", *Materials Science and Engineering: A*, Vol. 627, No. pp. 281-289 (2015)

Lin, H. C., C. A. Hsu, C. S. Lee, T. Y. Kuo, and S. L. Jeng, "Effects of zinc layer thickness on resistance spot welding of galvanized mild steel", *Journal of Materials Processing Technology*, Vol. 251, No. pp. 205-213 (2018)

Liu, Wei, Chuanjing Sun, Xiangyang Xu, Yinlong Zuo, and Jian Lin, "The influences of nugget diameter on the mechanical properties and the failure mode of resistance spot-welded metastable austenitic stainless steel", *Materials & Design*, Vol. 33, No. pp. 292-299 (2012)

Ma, C, DL Chen, SD Bhole, G Boudreau, A Lee, and E Biro, "Microstructure and fracture characteristics of spot-welded DP600 steel", *Materials Science and Engineering: A*, Vol. 485, No. 1-2, pp. 334-346 (2008)

Pouranvari, M, and SPH Marashi, "Failure of resistance spot welds: tensile shear versus coach peel loading conditions", *Ironmaking & Steelmaking*, Vol. 39, No. 2, pp. 104-111 (2012)

Pouranvari, M, HR Asgari, SM Mosavizadch, PH Marashi, and M Goodarzi, "Effect of weld nugget size on overload failure mode of resistance spot welds", *Science and Technology of Welding and Joining*, Vol. 12, No. 3, pp. 217-225 (2007)

Pouranvari, M, P Marashi, M Goodarzi, and H Bahmanpour, "Metallurgical factors affecting failure mode of resistance spot welds", *Mater. Sci. Technol*, Vol., No. pp. 2465-2473 (2008)

Pouranvari, M, SPH Marashi, and DS Safanama, "Failure mode transition in AHSS resistance spot welds. Part II: Experimental investigation and model validation", *Materials Science and Engineering: A*, Vol. 528, No. 29-30, pp. 8344-8352 (2011)

Pouranvari, Majid, "Effect of Welding Parameters on the Peak Load and Energy Absorption of Low-Carbon Steel Resistance Spot Welds", *ISRN Mechanical Engineering*, (2011)

Radakovic, DJ, and M Tumuluru, "Predicting resistance spot weld failure modes in shear tension tests of advanced high-strength automotive steels", *WELDING JOURNAL-NEW YORK-*, Vol. 87, No. 4, pp. 96-105 (2008)

Rao, Shravan Singh, Rahul Chhibber, Kanwer Singh Arora, and Mahadev Shome, “Resistance spot welding of galvannealed high strength interstitial free steel”, *Journal of Materials Processing Technology*, Vol. 246, No. pp. 252-261 (2017)
Sirinakorn, Thipwipa, Vitoon Uthaisangsuk, and Sompong Srimanosawapal, “Microstructure based Description of Deformation Behavior of Dual Phase Steel Sheets”, *Procedia Engineering*, Vol. 81, No. pp. 1366-1371 (2014)
Soomro, Imtiaz Ali, and Srinivasa Rao Pedapati, “Application of in situ post weld heat treatment using double pulse technology and its effect on microstructure and mechanical performance of resistance spot welded HSLA350 steel”, *The International Journal of Advanced Manufacturing Technology*, Vol. 105, No. 7-8, pp. 3249-3260 (2019)
Sun, Xin, Elizabeth V Stephens, and Mohammad A Khaleel, “Effects of fusion zone size and failure mode on peak load and energy absorption of advanced high strength steel spot welds under lap shear loading conditions”, *Engineering Failure Analysis*, Vol. 15, No. 4, pp. 356-367 (2008)
Vajragupta, N., P. Wechsuwanmanee, J. Lian, M. Sharaf, S. Münstermann, A. Ma, A. Hartmaier, and W. Bleck, “The modeling scheme to evaluate the influence of microstructure features on microcrack formation of DP-steel: The artificial microstructure model and its application to predict the strain hardening behavior”, *Computational Materials Science*, Vol. 94, No. pp. 198-213 (2014)
VandenBossche, D. J., “Ultimate Strength and Failure Mode of Spot Welds in High Strength Steels”, *SAE Transactions*, Vol. 86, No. pp. 955-966 (1977)
Xia, Mingsheng, Elliot Biro, Zhiling Tian, and Y Norman Zhou, “Effects of heat input and martensite on HAZ softening in laser welding of dual phase steels”, *ISIJ international*, Vol. 48, No. 6, pp. 809-814 (2008)
Zhang, Hongyan, and Jacek Senkara. 2011. *Resistance welding: fundamentals and applications*: CRC press.
Zhao, Yixi, Yansong Zhang, and Xinmin Lai, “Analysis of Fracture Modes of Resistance Spot Welded Hot-Stamped Boron Steel”, *Metals*, Vol. 8, No. 10, pp. 764 (2018)
Zhou, M, H Zhang, and SJ Hu, “Relationships between quality and attributes of spot welds”, WELDING JOURNAL-NEW YORK-, Vol. 82, No. 4, pp. 72-S (2003)

# 兩段脈衝電阻點銲對雙相鋼 DP980 之影響

李驊登　　張淵智
國立成功大學機械工程學系

## 摘 要

多段電阻點銲是汽車工業中一種與傳統單段電阻點銲不同的新方法。本研究中，針對單段和兩段電阻點銲製程進行了拉伸剪切試驗、銲點熔核大小、硬度分佈、微觀結構和不同銲接參數的失效模式等分析。實驗結果表明，兩段電阻點銲的熔核尺寸在所有實驗銲接電流均大於單段電阻點銲試件。而在較低的銲接電流之下，兩段電阻點銲的拉伸剪切負荷能力與破壞能均優於單段電阻點銲。但在較高的銲接電流之下，兩種銲接製程的拉伸剪切負荷能力和破壞能卻相同，這是因為較高的熱量輸入會引起軟化效應。硬度和微觀結構分析表明，銲件在部分熔化區和次臨界熱影響區出現軟化。破壞模式也取決於所施加的脈衝數。因此本研究發現，與單段銲接相比，兩段電阻點銲增加了軟化程度並改變機械性能，這是因為兩段製程中輸入的熱量更大，尤其是在銲接電流較高時。